Cortical oscillations arise from contextual interactions that regulate sparse coding

Monika P. Jadi[1] and Terrence J. Sejnowski[1]

Howard Hughes Medical Institute, Salk Institute for Biological Studies, La Jolla, CA 92037; and Division of Biological Sciences, University of California at San Diego, La Jolla, CA 92093

Contributed by Terrence J. Sejnowski, March 26, 2014 (sent for review November 30, 2013)

Precise spike times carry information and are important for synaptic plasticity. Synchronizing oscillations such as gamma bursts could coordinate spike times, thus regulating information transmission in the cortex. Oscillations are driven by inhibitory neurons and are modulated by sensory stimuli and behavioral states. How their power and frequency are regulated is an open question. Using a model cortical circuit, we propose a regulatory mechanism that depends on the activity balance of monosynaptic and disynaptic pathways to inhibitory neurons: Monosynaptic input causes more powerful oscillations whereas disynaptic input increases the frequency of oscillations. The balance of stimulation to the two pathways modulates the overall distribution of spikes, with stronger disynaptic stimulation (e.g., preferred stimuli inside visual receptive fields) producing high firing rates and weak oscillations; in contrast, stronger monosynaptic stimulation (e.g., suppressive contextual stimulation from outside visual receptive fields) generates low firing rates and strong oscillatory regulation of spike timing, as observed in alert cortex processing complex natural stimuli. By accounting for otherwise paradoxical experimental findings, our results demonstrate how the frequency and power of oscillations, and hence spike times, can be modulated by both sensory input and behavioral context, with powerful oscillations signifying a cortical state under inhibitory control in which spikes are sparse and spike timing is precise.

cerebral cortex | inhibitory interneurons | visual cortex model | gamma oscillations

Individual neurons can precisely time their spikes when driven by temporally fluctuating synaptic inputs (1). Narrowband oscillations mediated by inhibitory neurons are thought to be a key source of coordinated fluctuating discharges from input neurons, and they vary in power and frequency during wakeful behavior and sleep. Oscillations in the gamma range (30–80 Hz), thought to be mediated by fast-spiking inhibitory neurons expressing the calcium-binding protein parvalbumin (2, 3), are modulated by the sensory environment (4–6), attention (7), and volition (8), as well as by specific memory tasks, causing changes in sensory responses (2) and information transfer (3) in the cortex. The modulation is observed both in the oscillation power, which we define as the peak of a distinct "bump" in the power spectrum of the local field potential (LFP), as well as the oscillation frequency, which is the frequency at this peak in the power spectrum (5, 6). In current models of oscillations in neuronal networks, oscillations are regulated by stimulation of inhibitory neurons such that increasing stimulation mainly increases their frequency (9–11) or power (12). In the visual cortex, both the contrast and size of visual stimuli increase the stimulation to local inhibitory neurons (13, 14), but the former increases the frequency of gamma-range oscillations (6), and the latter decreases it (5). The power of gamma oscillations increases in the somatosensory, medial temporal (15), motor (8), olfactory (16), and primary visual cortex (5) with increased stimulation to local inhibitory neurons. However, the peak power of oscillations decreases with increased stimulation of inhibitory neurons with attention (17) in some cortical areas (7). In a third scenario, whereas the broadband power in the LFP signal increases with increasing visual contrast (6, 18), peak narrowband power shows no significant trend in response to increasing contrast (8), which is thought to increase the stimulation to the local inhibitory neurons (13).

We show that these diverse experimental observations can be explained by the following hypothesis: The balance of two distinct pathways that activate local inhibitory neurons mediates bidirectional regulation of oscillations (Fig. 1*A*). We classify these pathways as monosynaptic (MS), those that make direct excitatory synaptic connections to the inhibitory neurons, and disynaptic (DS), those that act through the local excitatory neurons.

Results

To test the hypothesis, we simulated a network of 800 excitatory and 200 inhibitory neurons with all-to-all connections (Fig. 1*A*). Individual neurons spiked stochastically with a probability determined by the integrated input from external sources and from other neurons in the network. Although stochastic spiking eliminated the potential for intrinsic oscillations in individual neurons, it allowed us to observe their spike trains in relation to the oscillating network. In addition to their synaptic action, the two types of neurons differed in how they responded to their integrated input, mimicking the excitatory pyramidal and inhibitory fast-spiking neurons that form the primary gamma-generating circuit in the cortex. To observe purely emergent fluctuations in the network, external excitation to the network was kept fixed in time.

Relative Strength of MS and DS Stimulation Determines the Power and Frequency of Oscillations. In response to sufficient stimulation of both the MS and DS pathways to inhibitory neurons, the fluctuations in the total spike rate of the network model showed robust narrowband oscillations (Fig. 1 *A* and *B*). As expected, individual neurons spiked irregularly, showing only a weak bias in their preferred spiking phase with respect to an oscillation cycle (Fig. S1). Oscillation frequency range in such a network depends on the strength of excitatory and inhibitory connections (19), and the network for the data shown here was tuned to

Significance

The nature and functions of oscillations in cerebral cortex are complex and controversial, and the mechanisms that regulate them are poorly understood. We propose a regulatory mechanism that links the dynamical state of the cortex to interactions between sensory and behavioral context during information processing. We explain how a prominent set of otherwise paradoxical empirical results can be understood with a single free parameter, the ratio of monosynaptic to disynaptic input to a subpopulation of inhibitory cells. In particular, we show that the power and frequency of gamma-range oscillations can be used to monitor the state of a cortical network. Our proposed model makes specific predictions that have broad implications for the basic understanding of information coding in the cortex.

Author contributions: M.P.J. and T.J.S. designed research; M.P.J. performed research; and M.P.J. and T.J.S. wrote the paper.

The authors declare no conflict of interest.

[1]To whom correspondence may be addressed. E-mail: jadi@salk.edu or terry@salk.edu.

This article contains supporting information online at www.pnas.org/lookup/suppl/doi:10.1073/pnas.1405300111/-/DCSupplemental.

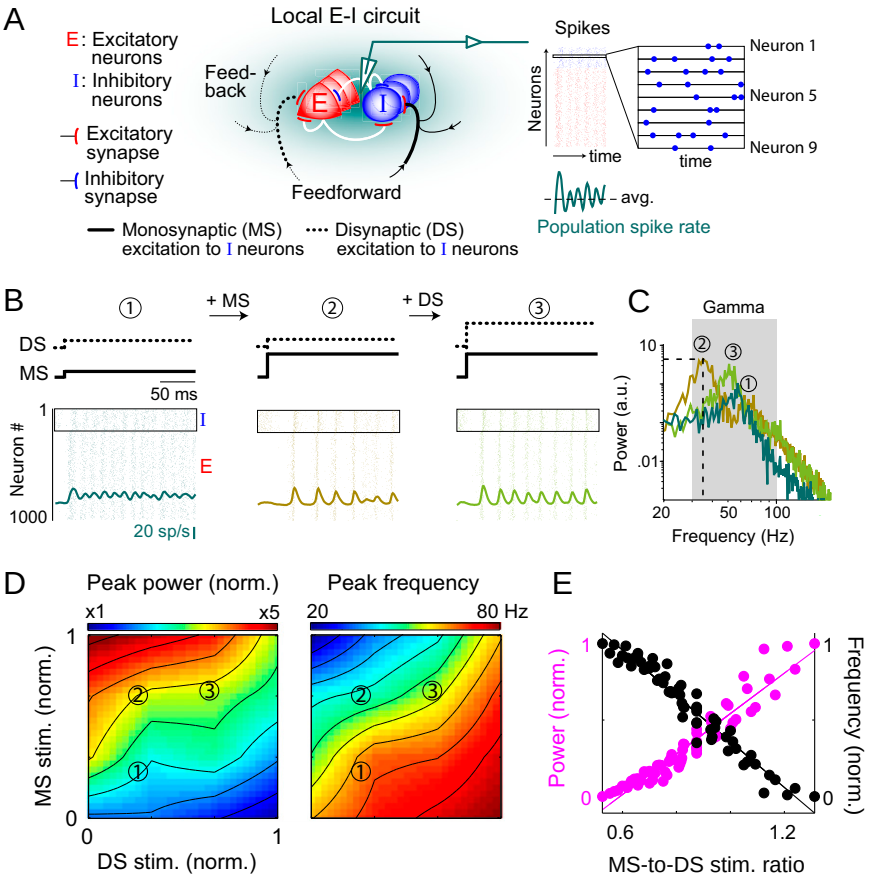

Fig. 1. Relative strength of MS and DS stimulation to inhibitory neurons determines the power and frequency of oscillations in spiking activity. (*A*) Schematic of local network and the monosynaptic (solid black) and disynaptic (dotted black) pathways for stimulating the local inhibitory neurons. The model network architecture featured both excitatory (E) and inhibitory (I) neurons, with recurrent connections between and within E and I populations. (*B*) Example evolution of population oscillatory activity (thick traces in green palette) from baseline (1) by increasing stimulation to MS (2) and DS (3) pathways in a model network oscillating in the gamma range (30–80Hz). The data shown are for first 200 ms of an example trial. The relative strengths of individual pathways are indicated at the top of each panel. Raster plots show the spike times of all inhibitory (inside rectangle) and excitatory neurons. (*C*) Power spectrum of average population activity for the three cases shown in *B* (mean across 10 trials of 2-s duration). Dotted lines indicate the peak power and corresponding frequency of narrowband oscillations. (*D*) Variation in peak power and frequency of narrowband oscillations with the strength of MS and DS stimulation of inhibitory neurons. The stimulation strengths are normalized to the range of interest. (*E*) Modulation of peak power and frequency of oscillations with the relative strength of MS-to-DS stimulation. The power and frequency data were normalized to the range of values shown in *D*. The MS-to-DS stimulation ratios were calculated from the absolute values of the two inputs used in the simulation experiments.

oscillate in the 30- to 80-Hz range. The power of oscillations was modulated by each stimulation pathway, but in opposite directions: It increased with increasing stimulation of the MS pathway and decreased with that of the DS one (Fig. 1 *B* and *C*). When the power of network oscillations increased, it was accompanied by a small but increased bias in the preferred phase of spiking for individual neurons (Fig. S1). The power of oscillations could be modulated bidirectionally over a range of external stimulation strengths (Fig. 1*D*), although the precise range was sensitive to the response properties of the two types of neurons (*Methods*). In addition, each pathway modulated the oscillation frequency, also in opposite directions: It decreased with increasing stimulation of the MS pathway and increased with that of the DS one (Fig. 1 *B*–*D*). When the pathways were comodulated, bidirectional control of both power and frequency was determined by the balance—both in its extent and direction of change—of stimulation to the two pathways; the repertoire of the model's behavior consisted of power-only (constant frequency lines in Fig. 1*D*) and frequency-only (constant power lines in Fig. 1*D*) as well as power-and-frequency modulations. In general, an increase in the ratio of MS-to-DS stimulation strengths resulted in more powerful but slower oscillations, and vice versa (Fig. 1*E*). Recent experiments suggest that slower gamma-range oscillations are induced by the recruitment of a spatially extended neural population (5, 20), an observation at odds with experimental evidence emphasizing the local nature of these oscillations (6, 21); our network demonstrates how a spatially limited neural population can generate both fast and slow oscillations.

Average Firing Rate Is Proportional to the Ratio of MS and DS Stimulation. Irregularity in the spiking of cortical neurons has been attributed to a balanced operating regime (22) wherein the net excitation and inhibition to an individual neuron varies in tandem. To characterize the operating regime of our network when driven by external input, we determined the mean excitatory and inhibitory spike rates for the entire range of MS and DS inputs that allowed bidirectional modulation of oscillations. When MS stimulation was increased, although the peaks of the fluctuating spike rates changed little (Fig. 1*B*), the mean spike rate for both excitatory and inhibitory population was reduced (Fig. 2*A*). However, when DS stimulation was increased, the mean spike rate for all the subpopulations went up. The extent of reduction or increase in the mean spike rates depended on the strength of the MS and DS pathways, respectively (Fig. 2*B*). Modulations of the excitatory and inhibitory spike rates had different sensitivities, but they were qualitatively similar (i.e., bidirectional across the entire range of stimulation strengths over which the network showed bidirectional regulation of oscillations). When the pathways were comodulated, change in mean spike rate was determined by the extent and direction of change in the balance of the stimulation to the two pathways (Fig. 2*C*).

Modulation of Oscillations Is Correlated with the Average Firing Rate of the Neuronal Population. The previous results demonstrated a regime of oscillatory regulation wherein increase in oscillation power is correlated with the reduction in average output spiking in the network, even for the inhibitory neurons (Fig. 3*A*): The larger the reduction of spike rate, the greater the increase in oscillatory power. Multiple studies of oscillations in the brain show a similar trend: stronger narrowband oscillations accompanied by sparser spiking activity (Fig. 3*B*, but see ref. 7), such as gamma-range oscillations in the medial temporal (15) and the primary visual cortices (5). In the motor cortex, which controls voluntary movement, amplification of gamma-range power through behavioral conditioning co-occurs with a weak reduction in local spike rates (8).

The results also demonstrated a regime of oscillatory regulation wherein the oscillation frequency is correlated with the output generated by the network, rather than the input to the inhibitory

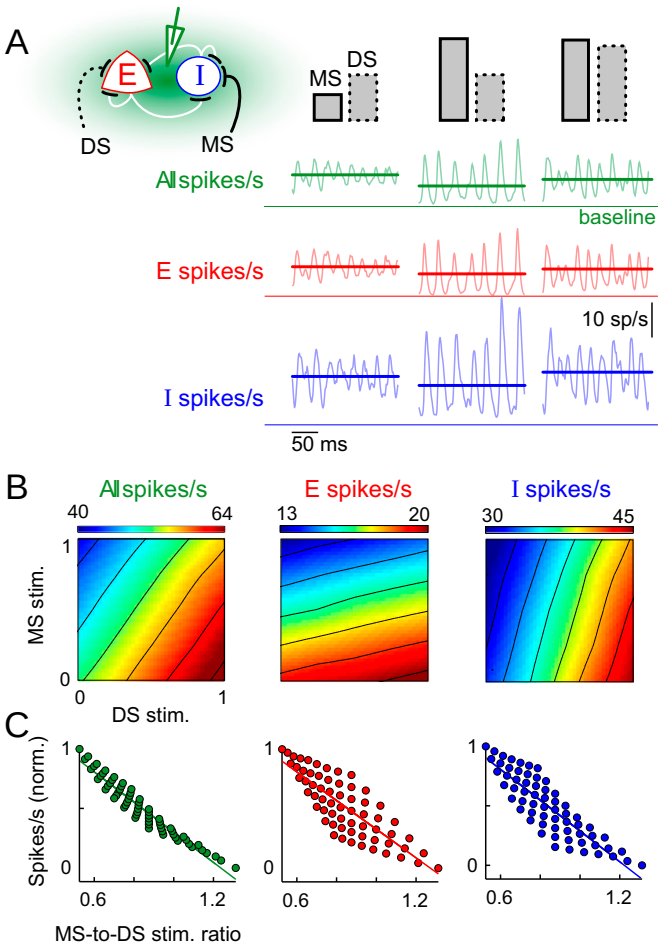

Fig. 2. The average firing rate is proportional to the ratio of MS-to-DS stimulation of inhibitory neurons. (*A*) Schematic on top left illustrates the MS and DS excitatory pathways to the inhibitory neurons in the network. The height of rectangles indicates the relative strength of stimulation to each pathway with respect to baseline. For the three cases indicated here, solid lines show the mean spike rate (spikes per second, calculated over 2 s of simulation) for the entire network (green), excitatory subpopulation (red), and inhibitory subpopulation (blue), with respect to baseline. Light-colored traces in the background show sample fluctuation of population spike rate for a trial of each scenario. (*B*) Heat plots of average spike rates as a function of the strength of MS and DS stimulation to inhibitory neurons. The mean activity was calculated by averaging over a 2-s trial. The data in the panel are average over 10 trials. (*C*) Modulation of mean spike rate of the network with the ratio of MS-to-DS stimulation. The spike rates for the total population (green) and the subpopulations (red and blue) were normalized to their respective ranges shown in *B*. The MS-to-DS stimulation ratios were calculated from the absolute values of the two inputs used in the simulation experiments.

neurons (Fig. 3*A*). The awake cortex indeed demonstrates such correlations: Peak frequency of gamma-range oscillations increases or decreases with a concomitant increase or decrease in the mean spike rate, respectively, in response to changes in sensory information (5, 6) or attention (6) (Fig. 3*B*).

Contrast-Dependent Modulation of Gamma Frequency and Local Network Activity. To corroborate these observations and also assay the effect of novel changes in the sensory environment on oscillation frequency, we simulated our network as a local neuronal network in the primary visual cortex (V1) with the following assumptions (Fig. 4*A*):

i) Visual stimuli in the classical receptive field (center)—the part of visual space that elicits maximal spikes at a V1 recording site when appropriately stimulated—strongly excite the DS pathway to the local inhibitory neurons; and

ii) Stimuli outside the classical receptive field (surround) strongly excite the MS pathway.

Assuming uniform selectivity of all the neurons for features of the visual input such as orientation, spatial frequency, and position in space, the input to the model V1 network was the visual contrast of a stimulus of fixed orientation (one preferred by the center) and fixed size. We increased the contrast of this visual input in three ways: (*i*) increase the contrast of the entire stimulus uniformly, (*ii*) increase the contrast of only the surround stimulus, with a fixed contrast at the center, and (*iii*) increase the contrast of the center stimulus to a lesser extent than that of the surround stimulus (Fig. 4*B*). In each case, the local V1 network showed oscillations in spike rates that were differently modulated by each contrast enhancement scenario. In the first case, frequency of oscillations increased with contrast (Fig. 4*C*). For the second case, the oscillations got slower as the contrast of visual stimulus increased. In the third case, the oscillation frequency remained unchanged when the contrast of visual stimulus increased. In all cases, the mean spike rate of the network changed in the general direction of change of the oscillation frequency. The predictions for only the first scenario of contrast modulation have experimental confirmation (6); the

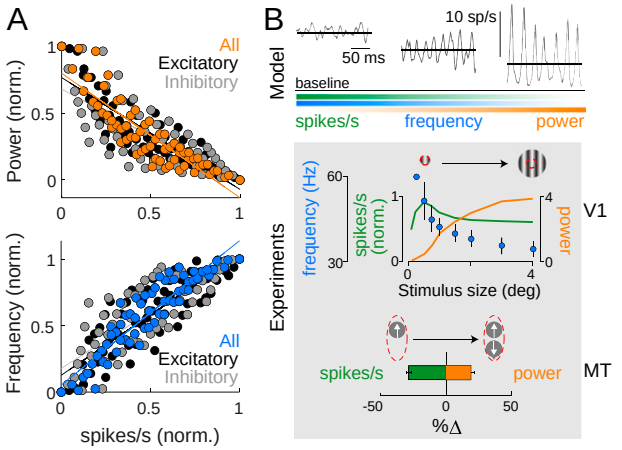

Fig. 3. Modulation of narrowband oscillations is correlated with the average spiking activity of the neuronal population. (*A*) Scatter plot of power (*Upper*) and frequency (*Lower*) in the population signal vs. the mean spike rate of (*i*) entire network (colored circles), (*ii*) excitatory subpopulation (black circles), and (*iii*) inhibitory subpopulation (gray circles). The normalized values were revisualized from data shown in Figs. 1*E* and 2*C*. (*B*) (*Upper*) Simulation of scenarios showing more powerful oscillations correlated with reduction of spiking activity. The average spike rate (solid black) was calculated over 20 s of simulation data, and example snippets of oscillatory fluctuations in spike rates are overlain in gray. Baseline spike rate was calculated over all trials across all scenarios. Fading bars schematically summarize the trend of spike rate, oscillatory power and frequency across the three cases. (*Lower*) V1: Electrophysiological data from the orientation-selective primary visual cortex (V1) of macaques during presentation of oriented stimuli. The plot shows mean spike rate (green), peak gamma-range frequency (blue), and peak gamma-range power (orange) as a function of increasing stimulus size [data estimated from Gieselmann and Thiele (5)]. The gamma power is plotted as a z-score. Red circle indicates boundary of receptive field in visual space of a V1 recoding site. MT: Electrophysiological data from the motion-selective medial temporal cortex (MT) of macaques during presentation of visual motion stimuli. The plot shows difference in mean spike rate (green) and peak gamma-range power (orange) between the cases when motion stimulus is presented in preferred direction alone (top left symbol) and when it is copresented with a motion stimulus in anti-preferred direction (top right symbol) [data estimated from Ray et al. (15)]. Red oval indicates boundary of receptive field of an MT recording site. Frequency data were not available.

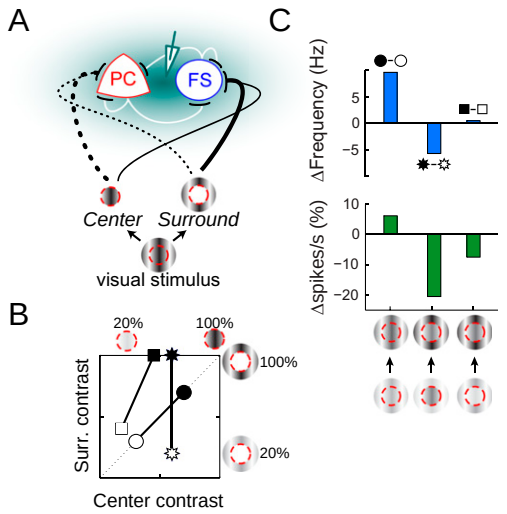

Fig. 4. Visual contrast-dependent modulation of gamma frequency and network activity in a model of the local network in the primary visual cortex (V1). (*A*) The schematic indicates the model assumptions for contribution (indicated by thickness of lines) of the visual contrast of different parts of a stimulus to the MS (solid) and DS (dotted) pathways to local inhibitory neurons in the V1. Red circle denotes boundary of the classical receptive field (visual space whose stimulation causes strongest spiking at a site in V1 tissue) of a V1 site. The cell labels PC (excitatory pyramidal cells) and FS (inhibitory fast spiking basket cells) denote cell types in the cortex with strong feedback connectivity and a role in gamma frequency oscillations (9, 10). They were implemented in the model as cells with different maximum spike rates. The model was tuned for gamma-range (30–100 Hz) oscillations. Visual contrast values were translated to MS and DS stimulation strengths using a linear transformation (*Methods* and Fig. S2). (*B*) Three types of contrast modulation of visual input were tested in the model: (*i*) uniform contrast modulation of the entire stimulus (circle), (*ii*) contrast modulation of surround only (star), and (*iii*) contrast modulation of the entire stimulus, but with center contrast increasing gradually compared to the surround (square). (*C*) Summary of oscillatory and average network activity in response to center and surround contrast modulation in the model. The panels show gamma-frequency and rate modulation for the scenarios described in *B*. The results show an increase, decrease, or no change in gamma frequency in response to increasing visual contrast depending on how it changes in different parts of the visual field.

model provides experimentally testable predictions for the other contrast modulation scenarios (*SI Notes: Predictions for Contrast Enhancement on Gamma-Range Frequency in Visual Cortex*).

Discussion

Oscillations are a signature of cortical information processing and their regulation is a reflection of the resulting neuronal code. Gamma-range oscillations recorded in vivo are modulated not only by the salience of the sensory input (6), but also by contextual information in the environment as well as internal brain state (5) and by volitional control (8). This suggests that the oscillations reflect the integration of bottom-up, lateral, and top-down information. A specific implication of this, for example, is that oscillation frequency in the sensory cortices will depend not only on the stimulus properties (6), but also on the sensory and behavioral context. The exploration shown here (Fig. 4) is a simpler version of such scenarios and illustrates the following point: Increasing just one aspect of sensory information (visual contrast in this case) can have a variety of effects on the oscillation frequency in a context-dependent way.

Population oscillations also narrow the spike times of individual neurons to specific phases in their cycle and improve spike synchrony (4, 8). Spikes are sparse and more precisely timed in our network when oscillations are more powerful (Fig. 3 and Fig. S1). In recordings from primary visual cortex, sparse and precisely timed spikes occur when wide-field dynamical natural movie stimuli are shown, but the spiking is more frequent and spike timing less precise when the same movie is restricted to the classical receptive field of a neuron (23). Thus, the same framework we propose for oscillatory regulation could address the regulation of spike synchrony, one of the coding strategies used in cortical function.

Normalization, a type of rescaling of neuronal spike rates, is considered a canonical computation in brain function and is implicated in several aspects of efficient neuronal coding (24), such as sparse representation of rich bottom-up sensory information (25, 26). Reduction in excitatory spiking by direct stimulation of local inhibitory neurons is one of the proposed neural mechanisms of this computation. A hallmark of this mechanism in the cortex is the paradoxical reduction in spiking of the inhibitory population (27), potentially those of the fast-spiking parvalbumin+ basket cells (28). In addition, electrophysiological recordings from several cortical areas show that normalizing sensory stimulation protocols that cause sparse spiking also results in more powerful oscillations (5, 15). Our work is the first demonstration to our knowledge of all three empirical observations within a single framework—sparse spiking of excitatory population, reduced spiking of inhibitory population, and more powerful network oscillations (Fig. 3 and Fig. S3)—in response to direct stimulation of the inhibitory population; it also provides the network mechanism that underlies these phenomena. Our work, along with electrophysiological data, suggests that power in oscillations codes the strength of normalization and powerful oscillations signify a sparse representation regime. Functional implications of such oscillations in the context of current theories of the role of normalization in information processing (25) need further investigation. Importantly, the predictions here pertain to regulation of cortical oscillations in general, and not specifically to gamma-range oscillations; the frequency in our model is strongly tied to the local connection strengths (19, 29), which can vary greatly between brain areas, causing oscillations with the same underlying mechanism but in different frequency bands. Indeed, experiments in the primary olfactory cortex show sparse neuronal responses, co-occurring with strong beta-range (20–30 Hz) oscillations during odor coding (16). Given the relatively sparse responses in motor cortex during volitional amplification of gamma-range synchrony, our work predicts that the amplification is mediated by a top-down normalizing pathway (8).

Our study offers a mechanism for the effect of attention on oscillation frequency and power in some cortical areas. Both spike rates and gamma-range oscillation frequency increase (6), whereas oscillation power decreases (7) in the primary visual cortex when attention is directed to sensory stimuli. Because such comodulation of firing rates, oscillation power, and oscillation frequency is also demonstrated by our network (Fig. 3*A*), it suggests that either an effective increase in the disynaptic input or an effective decrease in the monosynaptic one could mediate attention in such areas (Fig. 1*D*), the former being implicated by recent experimental data (30). In other cortical areas, such as visual area V4, a qualitatively different effect of attention on oscillation power in the same frequency range could be explained by fundamental differences between areas in terms of how attention is mediated (31) or the regulatory mechanism of oscillations itself.

Detectable stimulus-induced oscillations appear with a delay (~100 ms) in multiple cortical areas (5–7, 15). The experimental protocols in these studies involve simultaneous presentation of preferred and contextual stimuli that are necessary to induce oscillations. Our study proposes a simple relationship between the experimental protocol and latency of oscillations. Recurrent or top-down information flow in the cortex typically has longer latency than the feed-forward or bottom-up flow. If such information also happens to drive the MS pathway more effectively in the cortex, our network predicts a delay in powerful oscillations (Fig. 5). Indeed, in multiple cortical areas, contextual information can activate both recurrent and top-down pathways. The action is thought to be mediated by MS pathways to inhibitory neurons and is essential for observing powerful yet delayed oscillations (5, 6). The delay is comparable to the time it takes the local spiking activity to evolve in response to the additional contextual information (32). Our model predicts that when the contextual information is presented earlier, powerful oscillations should be detected earlier (Fig. 5). Because

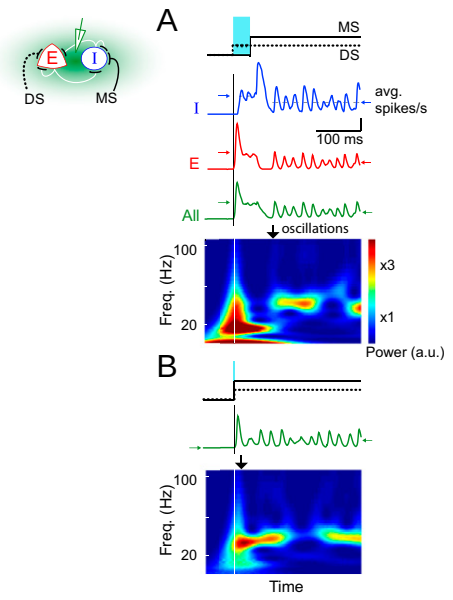

Fig. 5. Relative timing of DS and MS stimulation of inhibitory neurons determines onset of strong oscillations. (*A* and *B*) The top row indicates latency of MS stimulation relative to DS stimulation to the inhibitory neurons in the network. Light blue bar highlights the temporal offset between the two pathways. Colored traces show the fluctuations in population firing rates for an example trial (red, excitatory; blue, inhibitory; green, all). Horizontal arrows indicate the steady state average population activity before (left) and after (right) the onset of monosynaptic stimulation. Time-frequency plots below show spectral contents of the overall population activity for the example trial. Vertical lines mark the onset of DS stimulation. Black vertical arrows indicate the approximate onset of narrowband increase in power. Early activation of MS pathway resulted in earlier onset of powerful oscillations.

the natural sensory environment consists of rich contextual information at all times, earlier oscillations are more likely in such sensory experiences than in commonly used experimental protocols. Given that perception can take up to 150 ms after stimulus presentation (33), earlier emergence of oscillations could imply a functional role; the temporal order of sensory information could thus influence perception and other brain functions through its effect on narrowband oscillations (34).

Oscillations such as those in our model network arise from the interaction of local excitatory and inhibitory neural population, a mechanism referred to as PING (Pyramidal-Inhibitory neuron-Network-Gamma) (35). Although multiple phenomena may underlie the PING architecture itself (29), the noisy oscillations in our model are based on the phenomenon of limit cycles in an unstable regime of an inhibition-stabilized network (27). Elsewhere, we have used a rate model to further analyze the basis of the observed behavior in our spiking model from a dynamical systems perspective (36). An alternate model of narrowband increase in LFP power is based on quasi-cycles, which involve noise amplification of damped oscillations in the stable regime of the network (18, 29, 37, 38) and merits further investigation in the context of recent data on visual gamma. Predictions from multiple models such as those discussed in this study will be helpful in driving the next round of experiments on stimulus-induced oscillations.

Models of gamma oscillations based on synaptic delays (12) might not be ideal candidates for sensory areas given the evidence for highly localized circuitry involved in gamma generation (6): rapidly changing oscillation frequency following dynamic stimuli and different oscillation frequencies at nearby cortical sites. A model based on single neuron oscillations (39, 40) conflicts with the weak evidence for oscillations in neuronal spiking in pyramidal neurons (PN) (41) and mixed evidence for both regular and irregular spiking in inhibitory neurons (IN) (42). Although our model does not involve INs behaving as neuronal oscillators, given the much smaller proportion of INs in the cortex, it does suggest INs skipping fewer cycles of the network oscillations compared with the PNs. The fact that INs involved in the oscillations in our model, as well as in vivo (2, 3), fire at a higher rate than PNs could also explain the differential evidence for regularity of spiking of the two types of neurons during gamma. What we propose here was constrained primarily by stimulus-induced gamma as recorded in the visual cortex of primates. Gamma oscillations observed in different brain areas, in different species, and under different experimental conditions—in vivo vs. in vitro or stimulus-induced vs. pharmacologically induced—might not involve the same underlying phenomena. For example, it is possible that pharmacologically induced gamma in a slice recruits a different mechanism and is a different phenomenon than what is responsible for increased power in the LFP in the intact network in response to a sensory stimulus.

In conclusion, the regulatory mechanism explored in this study explains a wide range of data on the regulation of oscillations in the alert cortex interacting with the sensory world. It emphasizes the importance of contextual information, both sensory and behavioral, in addition to the signals that drive the classical receptive fields, in shaping these oscillations.

Methods

Network Description. A network of N_E excitatory and N_I inhibitory neurons was set up with connectivity depending only on the cell type. The synaptic weights between neuron types were as follows:

$$\text{E-to-E: } w_{EE} = \frac{W_{EE}}{N_E}$$
$$\text{I-to-E: } w_{EI} = \frac{W_{EI}}{N_I}$$
$$\text{E-to-I: } w_{IE} = \frac{W_{IE}}{N_E}$$
$$\text{I-to-I: } w_{II} = \frac{W_{II}}{N_I}$$

In a model cortical network made up of stochastic spiking neurons, we simulated $N_E = 800$ excitatory and $N_I = 200$ inhibitory neurons. In the simulations shown here, $W_{EE} = 16$, $W_{EI} = 26$, $W_{IE} = 20$, and $W_{II} = 1$. Although the connectivity for the results shown here was all-to-all, detailed treatment of general robustness of oscillations to a sparser connectivity pattern can be found elsewhere (29).

Stochastic Spiking Neurons. Individual neurons in the network were treated as coupled, continuous-time, two-state (active and quiescent) Markov processes (29) (*SI Methods*). The active state modeled a neuron's initiation of a spike followed by a refractory period, whereas the quiescent state modeled the neuron at rest. For the data shown here, the probability of excitatory and inhibitory neurons to transition to active state depended on the neuronal response functions described in Eq. **1**:

$$G_E(x) = \begin{cases} 0 & \text{for } x < \theta_E \\ m_E(x-\theta_E) & \text{for } \theta_E < x < \theta_E + 1/m_E \\ 1 & \text{for } x > \theta_E + 1/m_E \end{cases}$$
$$G_I(x) = \begin{cases} 0 & \text{for } x < \theta_I \\ m_I(x-\theta_I)^3 & \\ 1 & \text{for } G_I > 1. \end{cases} \quad [1]$$

In Eq. **1**, x is the integrated synaptic input to a neuron. This includes input from other neurons in the network as well as external input (see *SI Methods* for details). The external input is the disynaptic pathway in case of excitatory neurons and monosynaptic pathway in case of inhibitory neurons (Fig. 1*A*). Also in Eq. **1**, $m_E = 0.25$, $m_I = 0.005$, $\theta_E = 1$, and $\theta_I = 12$. The results were qualitatively unchanged when the network was simulated with different sensitivities m_E and m_I for these response functions. The range of inputs over which the network showed bidirectional modulation of power and frequency varied with the choice of response functions.

Simulation Environment. Network simulations, data analysis, and visualization were done in the MATLAB 2012a (The MathWorks) environment. An event-driven method was used for all simulations of the master equation (29). The simulation software was based on modification of a previously published method (29).

Data Analysis. The average activity was calculated from the simulation data by counting spikes in time bins of width 1 ms and convolving with a Gaussian of width 5 ms. The power spectrum of the average activity signal was calculated after removing the mean. The average power spectrum was estimated by taking a mean of power spectrum for 10 runs.

Data Visualization. The heat plots in Figs. 1*D* and 2*B* were visualized by linear interpolation for better visualization of the global trends in the simulation data.

Mapping Visual Contrast to MS and DS Drives. For simulation of the local E-I network in the primary visual cortex (Fig. 4), we mapped the effect of stimulus contrast on the drive to the MS and DS pathways as follows:

$$MS\_stim = \frac{0.01C + .3S}{160} + 0.4$$

$$DS\_stim = \frac{1.5C + .01S}{200} + 0.05,$$

where C and S were the visual contrast (in percentage) of the stimulus in the classical receptive field and surround, respectively.

ACKNOWLEDGMENTS. The authors thank Drs. A. Nandy, C. O'Donnell, and K. Padmanabhan for helpful comments on the manuscript. M.P.J. was supported by a National Eye Institute Training Grant NEI 2R01EY12872 and Howard Hughes Medical Institute (HHMI). T.J.S. was supported by HHMI.

1. Mainen ZF, Sejnowski TJ (1995) Reliability of spike timing in neocortical neurons. *Science* 268(5216):1503–1506.
2. Cardin JA, et al. (2009) Driving fast-spiking cells induces gamma rhythm and controls sensory responses. *Nature* 459(7247):663–667.
3. Sohal VS, Zhang F, Yizhar O, Deisseroth K (2009) Parvalbumin neurons and gamma rhythms enhance cortical circuit performance. *Nature* 459(7247):698–702.
4. Gray CM, König P, Engel AK, Singer W (1989) Oscillatory responses in cat visual cortex exhibit inter-columnar synchronization which reflects global stimulus properties. *Nature* 338(6213):334–337.
5. Gieselmann MA, Thiele A (2008) Comparison of spatial integration and surround suppression characteristics in spiking activity and the local field potential in macaque V1. *Eur J Neurosci* 28(3):447–459.
6. Ray S, Maunsell JHR (2010) Differences in gamma frequencies across visual cortex restrict their possible use in computation. *Neuron* 67(5):885–896.
7. Chalk M, et al. (2010) Attention reduces stimulus-driven gamma frequency oscillations and spike field coherence in V1. *Neuron* 66(1):114–125.
8. Engelhard B, Ozeri N, Israel Z, Bergman H, Vaadia E (2013) Inducing γ oscillations and precise spike synchrony by operant conditioning via brain-machine interface. *Neuron* 77(2):361–375.
9. Whittington MA, Traub RD, Jefferys JG (1995) Synchronized oscillations in interneuron networks driven by metabotropic glutamate receptor activation. *Nature* 373(6515):612–615.
10. Wang XJ, Buzsáki G (1996) Gamma oscillation by synaptic inhibition in a hippocampal interneuronal network model. *J Neurosci* 16(20):6402–6413.
11. Ermentrout GB, Kopell N (1998) Fine structure of neural spiking and synchronization in the presence of conduction delays. *Proc Natl Acad Sci USA* 95(3):1259–1264.
12. Brunel N, Wang X-J (2003) What determines the frequency of fast network oscillations with irregular neural discharges? I. Synaptic dynamics and excitation-inhibition balance. *J Neurophysiol* 90(1):415–430.
13. Atallah BV, Bruns W, Carandini M, Scanziani M (2012) Parvalbumin-expressing interneurons linearly transform cortical responses to visual stimuli. *Neuron* 73(1): 159–170.
14. Gilbert CD, Wiesel TN (1983) Clustered intrinsic connections in cat visual cortex. *J Neurosci* 3(5):1116–1133.
15. Ray S, Ni AM, Maunsell JH (2013) Strength of gamma rhythm depends on normalization. *PLoS Biol* 11(2):e1001477.
16. Poo C, Isaacson JS (2009) Odor representations in olfactory cortex: "Sparse" coding, global inhibition, and oscillations. *Neuron* 62(6):850–861.
17. Mitchell JF, Sundberg KA, Reynolds JH (2007) Differential attention-dependent response modulation across cell classes in macaque visual area V4. *Neuron* 55(1): 131–141.
18. Jia X, Xing D, Kohn A (2013) No consistent relationship between gamma power and peak frequency in macaque primary visual cortex. *J Neurosci* 33(1):17–25.
19. Wilson HR, Cowan JD (1972) Excitatory and inhibitory interactions in localized populations of model neurons. *Biophys J* 12(1):1–24.
20. Jia X, Tanabe S, Kohn A (2013) γ and the coordination of spiking activity in early visual cortex. *Neuron* 77(4):762–774.
21. Roelfsema PR, Lamme VA, Spekreijse H (2004) Synchrony and covariation of firing rates in the primary visual cortex during contour grouping. *Nat Neurosci* 7(9): 982–991.
22. van Vreeswijk C, Sompolinsky H (1996) Chaos in neuronal networks with balanced excitatory and inhibitory activity. *Science* 274(5293):1724–1726.
23. Haider B, et al. (2010) Synaptic and network mechanisms of sparse and reliable visual cortical activity during nonclassical receptive field stimulation. *Neuron* 65(1):107–121.
24. Carandini M, Heeger DJ (2012) Normalization as a canonical neural computation. *Nat Rev Neurosci* 13(1):51–62.
25. Schwartz O, Simoncelli EP (2001) Natural signal statistics and sensory gain control. *Nat Neurosci* 4(8):819–825.
26. Olsen SR, Wilson RI (2008) Lateral presynaptic inhibition mediates gain control in an olfactory circuit. *Nature* 452(7190):956–960.
27. Ozeki H, Finn IM, Schaffer ES, Miller KD, Ferster D (2009) Inhibitory stabilization of the cortical network underlies visual surround suppression. *Neuron* 62(4):578–592.
28. Adesnik H, Bruns W, Taniguchi H, Huang ZJ, Scanziani M (2012) A neural circuit for spatial summation in visual cortex. *Nature* 490(7419):226–231.
29. Wallace E, Benayoun M, van Drongelen W, Cowan JD (2011) Emergent oscillations in networks of stochastic spiking neurons. *PLoS ONE* 6(5):e14804.
30. Briggs F, Mangun GR, Usrey WM (2013) Attention enhances synaptic efficacy and the signal-to-noise ratio in neural circuits. *Nature* 499(7459):476–480.
31. Fries P, Reynolds JH, Rorie AE, Desimone R (2001) Modulation of oscillatory neuronal synchronization by selective visual attention. *Science* 291(5508):1560–1563.
32. Bair W, Cavanaugh JR, Movshon JA (2003) Time course and time-distance relationships for surround suppression in macaque V1 neurons. *J Neurosci* 23(20):7690–7701.
33. Thorpe S, Fize D, Marlot C (1996) Speed of processing in the human visual system. *Nature* 381(6582):520–522.
34. Eagleman DM, Jacobson JE, Sejnowski TJ (2004) Perceived luminance depends on temporal context. *Nature* 428(6985):854–856.
35. Tiesinga P, Sejnowski TJ (2009) Cortical enlightenment: Are attentional gamma oscillations driven by ING or PING? *Neuron* 63(6):727–732.
36. Jadi MP, Sejnowski TJ (2014) Regulating cortical oscillations in an inhibition-stabilized network. *Proc IEEE*, in press.
37. Bressloff PC (2010) Metastable states and quasicycles in a stochastic Wilson-Cowan model of neuronal population dynamics. *Phys Rev E Stat Nonlin Soft Matter Phys* 82(5 Pt 1):051903.
38. Kang K, Shelley M, Henrie JA, Shapley R (2010) LFP spectral peaks in V1 cortex: Network resonance and cortico-cortical feedback. *J Comput Neurosci* 29(3):495–507.
39. Börgers C, Kopell N (2003) Synchronization in networks of excitatory and inhibitory neurons with sparse, random connectivity. *Neural Comput* 15(3):509–538.
40. Ermentrout GB (1998) Neural networks as spatio-temporal pattern forming systems. *Rep Prog Phys* 61:353–430.
41. Pesaran B, Pezaris JS, Sahani M, Mitra PP, Andersen RA (2002) Temporal structure in neuronal activity during working memory in macaque parietal cortex. *Nat Neurosci* 5(8):805–811.
42. Hájos N, et al. (2004) Spike timing of distinct types of GABAergic interneuron during hippocampal gamma oscillations in vitro. *J Neurosci* 24(41):9127–9137.

Supporting Information

Jadi and Sejnowski 10.1073/pnas.1405300111

SI Methods

Stochastic Spiking Neurons. Individual neurons in the model were treated as coupled, continuous-time, two-state (active and quiescent) Markov processes (1). The active state represents a neuron firing an action potential and its accompanying refractory period, whereas the quiescent state represents a neuron at rest. The transition probability for the i^{th} neuron to decay from active to quiescent state in time dt was $P_i(active \rightarrow quiescent) = \alpha_i dt$, where α represented the decay rate of the active state of the neuron. Parameter α_i set the upper bound on firing rate of the stochastically spiking neuron, similar to refractory period. The transition probability for the i^{th} neuron to spike, that is, to change from quiescent to active state, was $P_i(quiescent \rightarrow active) = \beta_i G(S_i(t))dt$. This caused the firing probability to be a function of the input, with β_i as its peak value. Parameter S_i was the total synaptic input to neuron i, given as $S_i(t) = N_i(t) + I_i(t)$, where N_i was the net input from other neurons in the local network and I_i was the net external input to the neuron. The network input was $N_i(t) = \sum_j w_{ij} A_j(t)$, where w_{ij} are the weights of the synapses. The activity variable $A_j(t)$ was set to one (1) if the j^{th} neuron was active at time t and zero otherwise. The model neurons had no intrinsic capacity to oscillate because the interspike interval was the sum of two independent exponential random variables with parameters α_i and $\beta_i G(S_i)$, respectively. Excitatory (E) and inhibitory (I) neurons in the network were differentiated on the basis of two parameters of the model neurons: $\alpha_E = 0.04\ ms^{-1}$, $\alpha_I = 0.12\ ms^{-1}$ and $\beta_E = .4$, $\beta_I = .8$. The response function of transition probability of individual neurons was defined by the function described in *Methods*. The results in the main text were qualitatively unchanged when we changed the probability function to different nonlinearities as well as slopes. We used the Gillespie algorithm (2) [software implementation based on Wallace et al. (1)], an event-driven method of simulation, for all simulations of the master equation.

Conditions for Oscillations. Strong E-E and E-I connections were used for population-level oscillations to emerge in a model such as ours whose individual neurons show little oscillation in their spiking activity or in their rates. Comparable oscillation mechanisms have been studied elsewhere (1, 3, 4) to explain other aspects of narrowband oscillations such as the wide distribution of spiking phase with respect to the ongoing oscillations, cycle skipping, and low firing rates of individual neurons (5) in the cortex, characteristics that are robustly demonstrates by our model (Fig. S1).

SI Data Analysis

Spectrogram. The spectrograms (Fig. 5) were generated using the methods of wavelet transforms using a Morlet basis function. The wavelet transform coefficients were calculated using the Wavelet Toolbox in the MATLAB software. The frequency-to-scale mapping in the spectrogram was done by calibration via best frequency-to-scale match for a sine wave signal.

Spike Probability. The cyclo-histogram of spike probability as a function of gamma phase was calculated using simulation data of all 1,000 neurons in our network, at the peak frequency of gamma as calculated from the average power spectrum. The probability distribution was calculated with 20 s of simulation data over 50 phase bins.

SI Notes

Experimental findings (6) suggest that the center frequency of gamma oscillations increases with the contrast of a visual stimulus covering the classical receptive field (center) as well as extraclassical receptive field (surround). At the same time, experiments with increasing size of a visual stimulus suggest that the frequency decreases with the strength of surround suppression (7), a phenomenon of reduction in spikes rate by visual stimulation of surround. The strength of surround suppression also depends on the contrast of stimulus in the surround. This experimental evidence can be combined to propose a simple relationship for gamma-range frequency as a function of stimulus contrast as summarized in Eq. **S1**, where F and G are monotonically increasing functions of contrast. The center frequency of detectable gamma oscillations at the lowest contrast is the baseline frequency:

$$freq_{gamma} = freq_{baseline} + F(contrast_{center}) - G(contrast_{surround}). \quad \textbf{[S1]}$$

This predicts that increasing contrast of visual stimulus in the receptive field center makes the oscillations faster (6) and that of the receptive field surround makes them slower, as shown in the results in Fig. 4. Because uniformly covarying the contrast of center and surround results in a net increase in the gamma-range oscillation frequency (6), Eq. **S1** has to satisfy the condition in Eq. **S2**:

$$F(contrast) > G(contrast). \quad \textbf{[S2]}$$

Eqs. **S1** and **S2** predict that modulating the contrast of center and surround visual stimulus will have no effect on the gamma-range frequency if they are covaried such that they satisfy Eq. **S3**:

$$F(contrast_{center}) = G(contrast_{surround}). \quad \textbf{[S3]}$$

To get an intuition for the condition described by Eq. **S3**, we can derive it for a simple choice of functions F and G, as in Eq. **S4**, which coarsely approximates the experimental data and model predictions:

$$freq_{gamma} = freq_{baseline} + \overbrace{A \times contrast_{center}}^{F} - \overbrace{B \times contrast_{surround}}^{G}$$

where

$$A > B \ \ (\text{see Eq. } \textbf{S2}). \quad \textbf{[S4]}$$

The analysis predicts that frequency of gamma-band oscillations will remain unchanged if Eq. **S3** is satisfied. Substituting for F and G, the oscillation frequency will be unchanged if the contrasts of the visual stimulus in receptive field center and surround are covaried at a ratio less than 1 (one) (Eqs. **S4** and **S5**):

$$\frac{contrast_{center}}{contrast_{surround}} = \frac{B}{A}. \quad \textbf{[S5]}$$

The precise estimation of this ratio will require combining existing experimental data and that obtained from experiments suggested in Fig. 4.

1. Wallace E, Benayoun M, van Drongelen W, Cowan JD (2011) Emergent oscillations in networks of stochastic spiking neurons. *PLoS ONE* 6(5):e14804.
2. Gillespie DT (1977) Exact stochastic simulation of coupled chemical reactions. *J Phys Chem* 81(25):2340–2361.
3. Wilson HR, Cowan JD (1972) Excitatory and inhibitory interactions in localized populations of model neurons. *Biophys J* 12(1):1–24.
4. Brunel N, Wang X-J (2003) What determines the frequency of fast network oscillations with irregular neural discharges? I. Synaptic dynamics and excitation-inhibition balance. *J Neurophysiol* 90(1):415–430.
5. Pesaran B, Pezaris JS, Sahani M, Mitra PP, Andersen RA (2002) Temporal structure in neuronal activity during working memory in macaque parietal cortex. *Nat Neurosci* 5(8):805–811.
6. Ray S, Maunsell JHR (2010) Differences in gamma frequencies across visual cortex restrict their possible use in computation. *Neuron* 67(5):885–896.
7. Gieselmann MA, Thiele A (2008) Comparison of spatial integration and surround suppression characteristics in spiking activity and the local field potential in macaque V1. *Eur J Neurosci* 28(3):447–459.

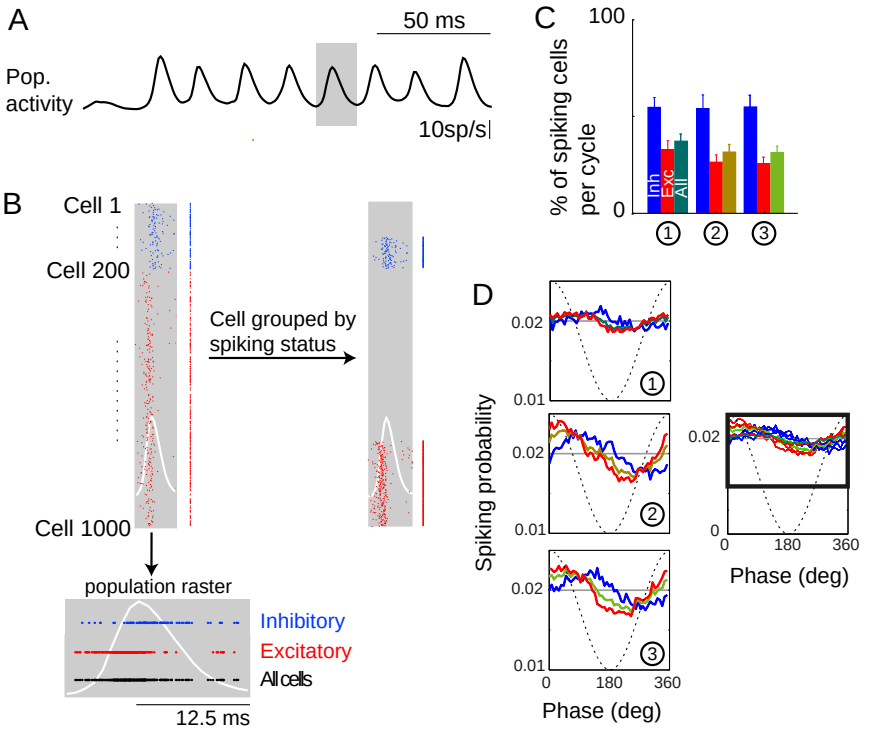

Fig. S1. Single neuron activity in the oscillating network. (*A*) An example trace of oscillations in population activity (total spikes per time bin) in the network. (*B*) Spike raster in a cycle of oscillating population activity in the trial shown in *A* (gray highlighted part of the trace). The population activity (white trace) is shown for reference. Gray rectangle in top left panel shows activity of all cells arranged by their IDs. Blue dots indicate activity of inhibitory cells and red dots indicated activity of excitatory cells. A time-collapsed version is shown on the side to illustrate active (colored dot) vs. nonactive (white space) cells in the particular oscillation cycle. Gray rectangle in top right panel shows the same raster with spiking cells grouped together to illustrate the fraction of cells active in an oscillation cycle. Gray rectangle in bottom left shows the same raster as multiunit activity for excitatory (red), inhibitory (blue), and whole population (green). (*C*) Fraction of neuronal population firing per oscillation cycle of the mean activity (red, excitatory; blue, inhibitory; green palate, all neurons). These statistics were calculated from 20 s of simulation data for each scenario shown in Fig. 1*B*. (*D*) Spike phase probability of all (green), excitatory (red), and inhibitory (blue) neurons as a function of the phase of ongoing oscillations. This was calculated with respect to the oscillation at peak frequency in the power spectrum of population activity, indicated by the dotted sinusoid. Solid gray line indicates a scenario when spikes occur at any phase of the ongoing oscillations with equal probability. Panel on the right shows the probabilities for all cases shown in Fig. 1*B*. Panels on the left zoom into the highlighted timescale in the panel on the right for each scenario in Fig. 1*B*.

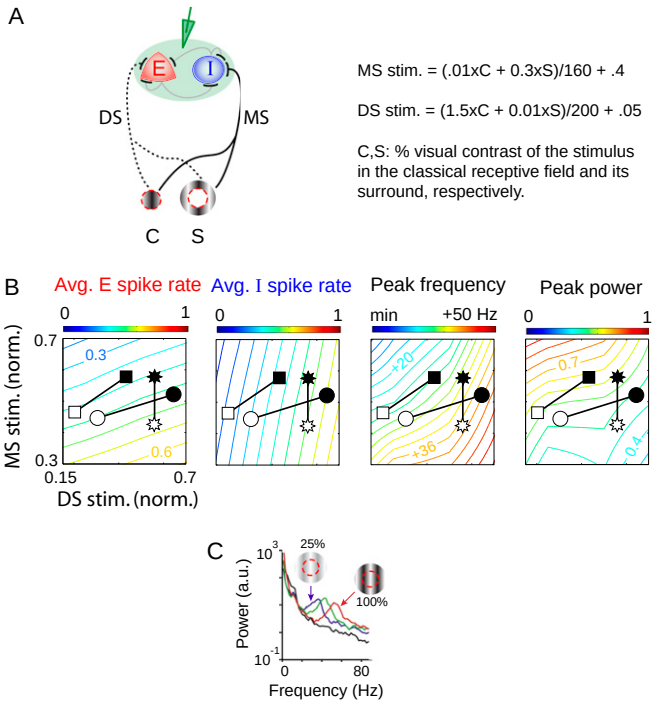

Fig. S2. Contrast dependence of gamma in visual cortex in model and experiments. (*A*) Linear translation formulae used to map the contrast of visual input described in Fig. 4*B* to stimulation of monosynaptic (MS) and disynaptic (DS) pathways in the model local visual cortical circuit. (*B*) Average spiking and oscillatory activity of neuronal population for the three scenarios of visual stimulation (indicated by three symbols) described in Fig. 4*B*. (*C*) Stimulus-induced gamma-range oscillations in the primary visual cortex increase their frequency with increasing contrast of the classical receptive field and its surround [adapted from Ray and Maunsell (6)]. The figure shows power in the local field potential signal at different frequencies.

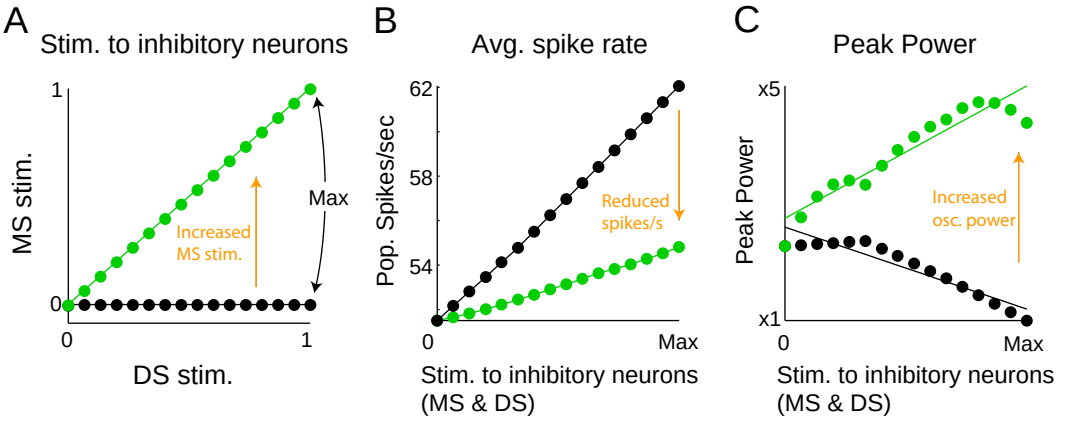

Fig. S3. Divisive normalization of spiking activity in the model network co-occurs with increased narrowband power. (*A*) An example of input scenarios leading to divisive normalization of the output spiking: increasing DS stimulation with weak/zero (black) and strong (green) stimulation to MS pathway in the model. The normalized stimulation units on the axes correspond to the ones shown in the main text Figs. 1 and 2. (*B*) Mean spike rates of the population in response to the two input scenarios shown in *A*. When the stimulation of MS pathway is increased with the DS pathway (green), the resulting population spike rates are scaled divisively compared with the scenario of weak MS stimulation (black). The data show average of 10 trials for each stimulation scenario. The *x* axis indicates combined increasing strength of stimulation (from 0 to maximum) to both MS and DS pathways for the scenarios described in *A*. **(C)** Power of peak narrowband oscillations in the population in response to the two input scenarios shown in *A*. When the stimulation of MS pathway is increased with the DS pathway (green), the resulting oscillation power is increased compared with the corresponding scenario of weak MS stimulation (black). The data show average of 10 trials for each stimulation scenario. The *x* axis indicates combined increasing strength of stimulation (from 0 to maximum) to both MS and DS pathways for the scenarios described in *A*.